Energy & Environmental Science

PAPER

View Article Online
View Journal | View Issue

Cite this: *Energy Environ. Sci.*, 2014, **7**, 3026

3D printed flow plates for the electrolysis of water: an economic and adaptable approach to device manufacture

Greig Chisholm, Philip J. Kitson, Niall D. Kirkaldy, Leanne G. Bloor and Leroy Cronin*

Received 8th May 2014
Accepted 24th June 2014

DOI: 10.1039/c4ee01426j

www.rsc.org/ees

The electrolysis of water is considered a promising route to the production of hydrogen from renewable energy sources. Electrolysers based on proton exchange membranes (PEMs) have a number of advantages including high current density, high product gas purity and the ability to operate at high pressure. Despite these advantages the high cost of such devices is an impediment to their widespread deployment. A principal factor in this cost are the materials and machining of flow plates for distribution of the liquid reagents and gaseous products in the electrochemical cell. We demonstrate the production and operation of a PEM electrolyser constructed from silver coated 3D printed components fabricated from polypropylene. This approach allows construction of light weight, low cost electrolysers and the rapid prototyping of flow field design. Furthermore we provide data on the operation of this electrolyser wherein we show that performance is excellent for a first generation device in terms of overall efficiency, internal resistances and current–voltage response. This development opens the door to the fabrication of light weight and cheap electrolysers as well as related electrochemical devices such as flow batteries and fuel cells.

Broader context

Uptake of renewable energy generation, especially wind and solar power is increasing at a dramatic rate and has the potential to contribute greatly to mankind's management of climate change due to accumulation of CO_2. Matching supply and demand of these intermittent renewable energy sources is challenging and solutions offered often depend on the conversion of excess electrical power to chemical or potential energy for storage until required. Hydrogen is a potential storage medium in this regard and the use of polymer electrolyte membrane (PEM) electrolysers holds great promise for the generation of hydrogen from renewable sources. Successful realisation of this goal requires product development of all parts of the PEM electrolyser from the "active" components *e.g.* the catalysts, to the "passive" components, namely the structural parts of the electrolyser stack. 3D printing is an emerging technology which can be used in the fabrication of many different device types. Here we present the use of 3D printing to prepare components of an electrolyser cell and demonstrate its operation. This application of 3D printing enables rapid prototyping, cost reduction and a dramatic reduction in component weight. All of which may accelerate the development of new electrolyser technologies.

Introduction

The proton exchange membrane (PEM) electrolysis of water was first described in the mid-1960s by General Electric as a method for producing oxygen for the Gemini Space Program and is now an established technology for the splitting of water into hydrogen and oxygen.[1] In recent years this technology has received significant attention as a potential route to the production of hydrogen from renewable energy sources.[2] PEM electrolysers have a number of advantages compared to the more established alkaline electrolysis process, namely production of hydrogen at a higher purity,[3] increased charge density on the electrodes leading to faster gas evolution,[4] and the ability to operate at pressures up to 200 bar thus reducing the need for compression of the product gas for storage.[5] These factors all contribute to the promotion of PEM based electrolysis as a cornerstone for the supply of hydrogen in a "hydrogen economy".

PEM electrolysers follow a standard design illustrated in Fig. 1. The principal components of the electrolyser are (i) the membrane electrode assembly consisting of a proton permeable membrane, often Nafion®. Each side of this membrane is coated with a suitable electrocatalytic substance to accelerate the electrolysis process. (ii) Porous gas diffusion layers (GDL) – often made of titanium or carbon which transfer current from the flow plates and promote the release of the product gases from the electrolysis reaction. (iii) Flow plates which separate each cell in the electrolyser stack and which are machined with a flow path for circulation of the water.

PEM electrolysers are more expensive than their alkaline counterparts and this, in part has limited their application, with

School of Chemistry, University of Glasgow, Glasgow, G12 8QQ, UK; Web: http://www.croninlab.com/. E-mail: Lee.Cronin@Glasgow.ac.uk

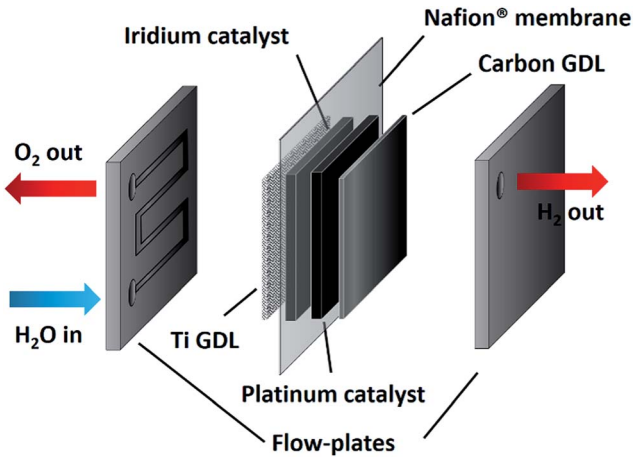

Fig. 1 Electrolysis cell construction.

considerable research being undertaken to reduce the costs of these devices, principally by reduction of catalyst cost by substitution of the noble metal catalysts for cheaper and more readily available alternatives.[6] Ayers *et al.* reported that the bipolar plate assembly is the highest cost component in the stack, representing nearly 40% of the overall cost.[7] These plates also contribute to the overall resistance of the cell and thus to the required cell voltage. This effect is more pronounced at the high charge densities at which PEM electrolysers operate and is one of the dominating sources of cell efficiency. These plates are also essential in the mass transport of both the reacting liquid (water) and the extraction of the product gases away from the membrane and the current collectors. Currently flow plates are typically made from graphite, titanium or stainless steel.[4] Each of these materials has its own advantages and disadvantages. Titanium is characterized by its high strength, high electrical and thermal conductivity and its low gas permeability, all of which are positive traits for a flow plate. The drawback of titanium is its relatively poor corrosion resistance, especially on the anodic side where an oxide layer can form, increasing the resistance and lowering the performance of the stack over time.[8] Graphite, whilst having high conductivity, suffers from poor corrosion resistance, limited mechanical strength and high cost.[8] Various grades of stainless steel may be employed.[9] This is a cheaper alternative to both titanium and graphite, however the stainless steel can corrode quickly in acidic environments and can require the application of a protective coating to reduce this corrosion to acceptable levels, but this can increase the resistance of the flow plate.[4] Considering all of the above, there is no ideal material for the construction of the PEM electrolyser flow plates.

Within the design of the flow plate, another aspect to consider is the effect of different configurations of the channels distributing the water and conducting the product gases away from the reaction sites. Possible configurations include pin-type flow fields,[10a] straight flow fields,[10b] serpentine flow fields,[10c] integrated flow fields,[10d] and interdigitated flow fields.[11] Considering the costs and time required to machine flow plates of a suitable material, detailed studies of the effect of the flow plate configuration on the performance of the electrolyser are lacking and performance testing is often carried out on a single configuration due to cost and time constraints.[12] An additional consideration in the manufacture of PEM electrolysers is the weight of the system which is largely influenced by the heavily engineered flow plates, current collectors and any further engineering required to render the electrolyser safe and stable particularly during high pressure operation.[13]

3D printing is an emerging technology which promises to revolutionize many areas of manufacturing processes, transforming the relationships between the design, manufacture and operation of functional devices.[14] In recent years there has been considerable interest in 3D-printing technologies for large-scale industrial prototyping,[15] and the manufacture of bespoke electronic[16] and pneumatic devices.[17–19] Considerable progress has been made in demonstrating the utility of 3D printing in the chemical sciences in the "reactionware" series of publications.[20–22] Herein we explore the revolutionary device fabrication potential of 3D printing applied to the aforementioned challenges of the design and manufacture of electrolyser components, resulting in a new manufacturing paradigm wherein 3D printed components are, for the first time, incorporated into an electrolyser.

Results and discussion

Preparation and characterisation of 3D printed flow plates

Fabrication of the flow plates was carried out using a Bits from Bytes 3DTouch™ 3D printer using a layer by layer deposition method. The plates were fabricated from polypropylene. Two coats of silver paint were applied to the polypropylene flow plate, curing at 120 °C after each coat had been applied and allowed to dry at ambient conditions. It was found that this silver coating adhered better if the flow plates were thoroughly cleaned in detergent solution with ultrasound prior to application of the paint. Failure to do this often resulted in areas of the coating delaminating from the polypropylene surface during curing. After coating with silver paint the flow plates were considered suitably conductive for electrocoating. The process of Polk *et al.*[23] was adopted for the coating process wherein a solution of 0.3 M $AgNO_3$ in 1 M NH_3 is used as the electrocoating media. The final thickness of the coated layer was 300 μm.

The electrical resistance of the flow plates decreased with each stage of the coating process. Average resistances measured during the fabrication of 3 plates are given in Table 1. We believe that the large standard deviations at each stage of the coating process are due to variations in the thickness of the layers applied by painting. Alternative methods of applying

Table 1 Electrical resistance of coated flow plates

	Coat 1	Coat 1 – cured	Coat 2	Coat 2 – cured	Electro-dep.
Av. R (Ω)	7.187	1.924	0.849	0.519	0.002
Std. dev.	5.441	1.271	0.311	0.144	0.002

these initial silver layers that may reduce this variation will be the subject of future work. For comparison, a variation of 0.002 Ω in the ohmic region of the polarisation curve would equate to an additional 26 mV or 1% of the total voltage required to drive the electrolysis at the maximum charge density. As shown in Table 1, after electrocoating with silver, flow plates with extremely low resistance can be obtained, however the performance of these plates in the electrolyser quickly deteriorated. This was due to oxidation of the silver on the anode during water electrolysis which resulted in silver ions that were able to migrate through the Nafion® membrane to the reductive side of the cell where they were reduced back to silver resulting in both an increase in the resistance of the anodic flow plate and irreversible damage to the Nafion® membrane. This production of silver within a Nafion® membrane is known and is exploited in the preparation of silver nanoparticles.[24] In order to prevent this oxidation of the anodic flow plate, a layer of gold was sputter coated onto the silver surface. This rendered the anodic flow plate inert to oxidation. The resistance of the plates was unchanged after sputter coating.

Photographic and SEM images of the flow plates at different stages of their preparation are given in Fig. 2. All SEM images were recorded at ×1000 magnification and the scale bar corresponds to 50 μm. Fig. 2a shows the polypropylene plate immediately after printing was complete and prior to application of any coating. Fig. 2b shows the flow plate after application of both layers of silver paint. The overlapping flakes of silver can be clearly observed. Contrast this with the appearance after electrodeposition of the silver (Fig. 2c) where layers of large crystallites of silver can be observed. This dense crystallite structure gives rise to the significant reduction in resistance observed between the cured 2nd coating of silver paint and the electrodeposited layer. The weight of the coated 3D printed flow plate was compared with the weight of a flow plate fabricated from titanium using an identical design. Both flow plates were 3 mm thick. The 3D printed flow plate was substantially lighter, weighing only 13.9 g whereas the titanium flow plate weighed 59.2 g, more than 4 times as much. This is extremely significant when one considers the number of flow plates that would be assembled in a stack.

The costs of the components were compared using the following market values: titanium $13.53 per kg;[25] polypropylene $1.54 per kg [26] and silver $620 per kg.[27] Using the weights above this gives a materials cost for the titanium plate of $0.80 per plate, compared with $0.17 per plate for the 3D printed component, a cost which includes the deposition of 0.25 g of silver. This amount of silver is typical of that deposited at the current used during electrocoating.

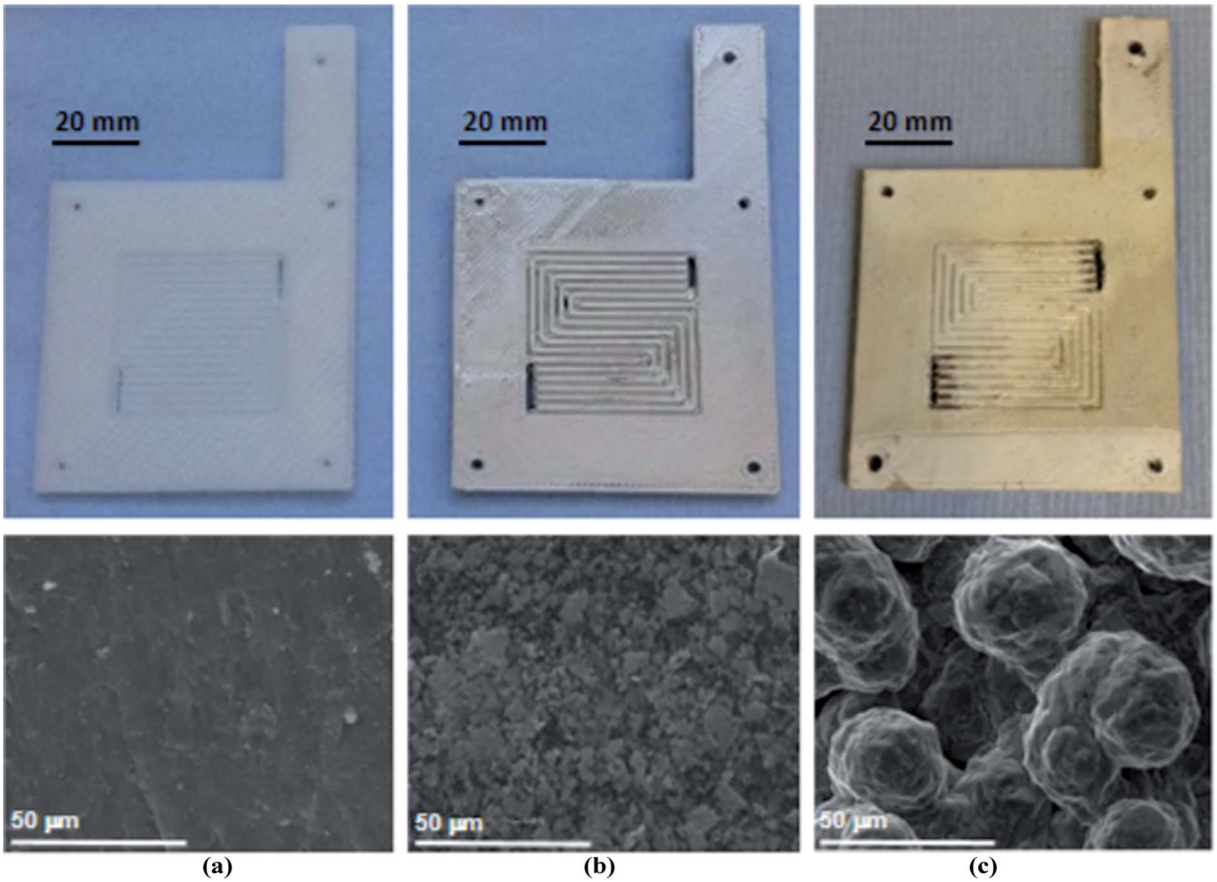

Fig. 2 Photographs and corresponding SEM images of polypropylene flow plates during various stages of coating. (a) Uncoated polypropylene. (b) After curing of the 2nd coat of silver paint. (c) After electrodeposition of silver.

Polarisation curves and efficiency

The relationship between current and voltage is critical to assessing the performance of an electrolyser. The current will increase with increasing voltage. Both the rate at which the current increases with each voltage step and the onset voltage of the electrolysis reaction are important measures of performance. A low onset voltage is indicative of an effective catalytic coating in the membrane electrode assembly whereas a rapid increase in the current is associated with good electrical contact between the components of the cell resulting in a low resistance.

Polarization curves were collected for the 3D printed cell at temperatures of 30, 50 and 70 °C and are illustrated in Fig. 3.

Onsets for water splitting are determined by extrapolation of the ohmic (linear) region of the polarisation curve. The onset of water electrolysis varied slightly with temperature: at 30 °C onset was 1.61 V, at 50 °C onset was at 1.57 V, and at 70 °C onset was at 1.54 V. The maximum current density achieved at 2.5 V and 30 °C was 1.04 A cm^{-2}. This increased when the temperature was increased to 50 °C, where a current density of 1.09 A cm^{-2} was reached. There was no further improvement in the performance of the cell when the temperature was increased to 70 °C. Temperatures greater than 70 °C were not investigated to avoid dehydration of the Nafion® membrane.

The limiting of the performance with increasing temperature is surprising as a standard electrolyser will achieve progressively higher current densities at a given voltage as the temperature increases. We believe that this limitation in performance can be explained by comparing the linear thermal expansion coefficients of the polypropylene substrate and the topmost silver layer. The linear thermal expansion coefficient of polypropylene varies with temperature from 1×10^{-4} to 2×10^{-4} K^{-1} depending on temperature.[28] This is 5–10 times the value for silver (1.9×10^{-5} K^{-1}).[29] Given this expansion of the polypropylene layer it is likely that this induces a distortion in the silver coating, increasing the distance between the particles and/or decreasing the extent of overlap. This will have the effect of increasing the resistance of the flow plate and effectively cancelling out the expected improvement in performance at a higher temperature.

The Faradaic and energy efficiencies of the cell were recorded at 30 °C, 2 V and 0.39 A cm^{-2}. The Faradaic efficiency was 94% and the energy efficiency was 70%. The 6% Faradaic loss may be due to parasitic electrochemical processes occurring within the flow plates, especially within the binder used in the silver paint.

Electrochemical impedance spectroscopy (EIS)

Applying a direct current to an electrolysis cell results in an overall cell voltage, V_{cell}, which can be described by eqn (1).

$$V_{cell} = V_{rev} + V_{ser} + V_{pol} + V_{con} \quad (1)$$

This equation describes the overall cell voltage, V_{cell} as the sum of four components. V_{rev} is the reversible voltage and is the minimum voltage required for electrolysis to take place. This is a function of the enthalpy of water and assumes no overpotentials or resistances and all reagents and products being in the gas phase. The remaining voltages can be considered as inefficiencies which the cell operation and design attempt to address. V_{ser} corresponds to the voltage drop associated with the resistance of the various cell components *e.g.* the membrane, the electrodes and the quality of the connection between these components. This connection is most often optimised by varying the torque on the bolts that maintain the integrity of the cell. V_{pol} is related to the voltage drop associated with the activation energy of the oxygen and hydrogen evolving reactions. V_{con} is due to mass transfer effects, namely the production of product gases at the electrodes and their efficient removal such that sufficient reactant can continue to be supplied to maintain a given charge density. Electrochemical impedance spectroscopy allows us to probe the resistances associated with these overpotentials in particular V_{ser} and V_{pol}. The Nyquist plots for the 3D printed cell are given in Fig. 4.

The series resistance (R_s) was largely constant at all temperatures, ranging only from 0.73–0.75 Ω cm^2. The polarization resistance (R_p) spanned the range 1.87 Ω cm^2 at 30 °C to

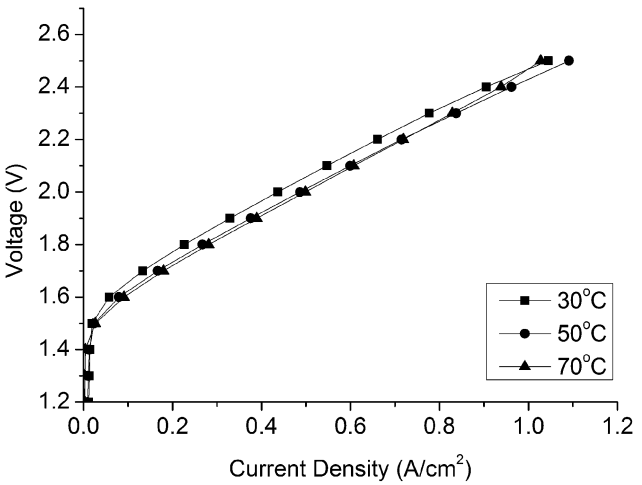

Fig. 3 Polarisation curve for water electrolysis in 3D printed electrolyser.

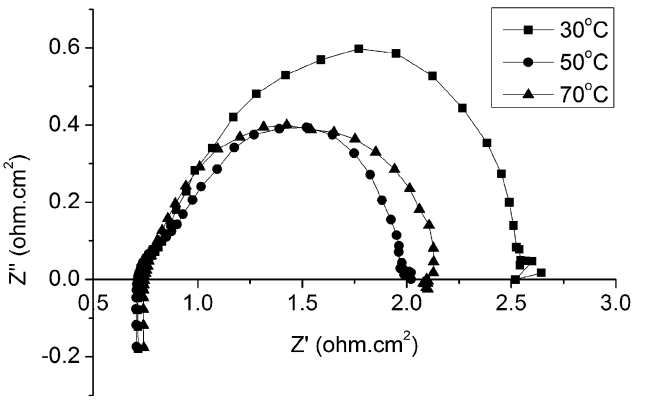

Fig. 4 Impedance Spectroscopy for water electrolysis using 3D printed electrolyser.

1.38 Ω cm^2 at 70 °C. The minimum value was reached at 50 °C, where R_p was 1.30 Ω cm^2. The EIS results agree well with those obtained from the polarisation curves. The fact that the EIS curve is largely unchanged between 50 and 70 °C is reflected in the similarities between the polarisation curves at these temperatures. Although typically a lesser effect *versus* the reduction in polarisation resistance with increasing temperature, the series resistance is also typically observed to drop. This does not occur in our cell and is possibly due to the thermal expansion of the polypropylene layer as previously discussed.

Durability

Our principal concern regarding the durability of the cell related to the performance of the anode, wherein the silver is prone to oxidation, leading to degradation of the performance of the cell. In order to assess this durability, an electrolysis cell was constructed consisting of a 3D printed flow plate for the anode and a 3 mm thick titanium flow plate for cathode. In other respects, the cell was identical to that used for all previous experiments. The voltage response of the cell was recorded over 96 hours at a constant current density of 0.25 A cm^{-2}. The results are illustrated graphically in Fig. 5.

During the 96 h duration of the experiment, the performance of cell decreases by an average of 2.1 mV h^{-1}, however this does not fully describe the behaviour or the stability of the cell over this time. The durability of the cell is characterised by 3 distinct phases. During the first hour of operation there was a marked decline in performance of 161.2 mV. After this initial degradation, the cell enters a period of comparative stability where the performance degrades at 1.0 mV h^{-1}. This phase lasts for approximately 26 hours. Thereafter the cell becomes even more stable degrading at only 0.14 mV h^{-1} for the remaining 70 hours of the experiment. The reason for these distinct rates of degradation are not known, however they are likely to be associated with electrochemical degradation of the binder components of the silver paint and oxidation of any exposed silver crystallites and concomitant degradation of both conductivity and membrane performance.

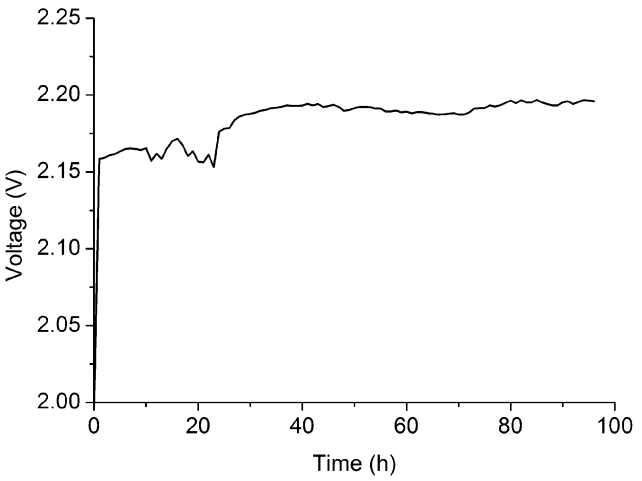

Fig. 5 Durability of 3D printed electrolyser.

Experimental

Flow plate fabrication

The 3D-printed flow plates used in this work were designed on the freely distributed 3D CAD software Autodesk123D (http://www.123dapp.com/) although any 3D modelling/CAD software with the ability to export models in a .STL file format would suffice for this, and there are a number of suitable alternative free/open source candidates available on the internet. The device designs were exported as .STL files (available from the authors), which was then interpreted by Bits from Bytes Axon 2 software to produce a 3D printer instruction file (.bfb file). This was subsequently transferred to the 3dTouch™ 3D printer. The printing was conducted in a layer-by-layer fashion by the 3dTouch™ printer, and the devices were printed using polypropylene (PP). The 3D printer used in this work had a print tolerance of ±0.2 mm in the *X* and *Y* directions and the *Z* resolution (*i.e.* the height of each layer of deposited thermopolymer) of the printer was 0.125 mm (±0.06 mm). The printed flow plates took approximately 2.5 hours to print. The active area of the flow plates, *i.e.* the area in contact with the catalyst is 12.96 cm^2. The flow channels are 0.9 mm deep and 0.9 mm wide.

Flow plate coating

Flow plates were ultrasonically cleaned in detergent solution for 10 minutes. The surface of the flow plate containing the channels was then painted using silver conductive paint (RS components; product no. 186-3600). The paint was allowed to air dry for one hour before being cured at 120 °C for 20 minutes. A second coat was applied and cured in the same manner. Electrocoating was carried out using the procedure of Polk *et al.*[23] Plating onto clean electrodes was accomplished from 0.3 M $AgNO_3$ in 1 M NH_3 by using a three-electrode cell at room temperature. A silver wire served as reference electrode, and a platinum gauze served as the counter electrode. Plates were coated for 1000 s at 1.0 V. Typical currents observed were 200 mA. Sputter coating was carried out using a BioRad SC510 sputter coater equipped with a gold target. Coating was carried out in an argon plasma at 1.5 kV, 20 mA and for 585 s, giving rise to a coating of approximately 1.04 μm. Thickness of the coatings were measured by delamination of the coating from the polypropylene substrate by heating to 120 °C and bending the flow plate. The thickness of the resultant flakes was measured using digital callipers, accurate to ±30 μm. Resistances of the flow plates were measured *via* impedance spectroscopy and were carried out using a Bio-Logic SP-150 potentiostat equipped with a VMP3B-20 20A booster. Data was collected and analysed using EC-Lab (v10.36) software. Measurements were carried out at 0 V *versus* reference at a frequency of 100 kHz and a sinus amplitude of 20 mV. The uncompensated resistance (R_u) is quoted.

Electrochemical cell construction

The configuration of the cell is given in Fig. 1. The interface between the flow plate and the Nafion membrane was gasketed with 0.12 mm PTFE (anode) and 0.15 mm Klinger (cathode) gaskets. The stack compression was 7.5 Nm. Deionised water

was supplied to the anode of the cell at a flow rate of 10 ml min^{-1}. The temperature in the cell was controlled by heating the deionized water reservoir in a water bath. The temperature of the feed water was measured by K-type thermocouples inserted into the feed water reservoirs. Temperature data was recorded using a Pico TC-08 data logger and PicoLog for Windows v5.22.1 (Pico Technology Ltd.).

Electrochemical characterization

Measurement of the current density as a function of cell potential, and electrochemical impedance spectroscopy (EIS) were carried out using a Bio-Logic SP-150 potentiostat equipped with a VMP3B-20 20A booster. Data was collected and analysed using EC-Lab (v10.36) software. Impedance spectroscopy measurements were carried out with potentiostatic control, in single sine mode and sweeping from 20 kHz to 0.1 Hz. The amplitude of the excitation signal was 0.01 V. The series resistance was determined from the intercept of the Nyquist plot with the real axis. The polarization resistance was calculated from the difference between the low and high frequency intercepts on the real axis. Curves were fitted using the equivalent circuit $L_1 + R_1 + Q_2/R_2$, where L_1 represents an inductor, R_1 is the series resistance of the cell (R_s), R_2 is the polarisation resistance of the cell (R_p) and Q_2 represents a constant phase element. Optimisation of the fitted curve was achieved using a randomise followed by a simplex curve fitting strategy. Weighting was set at 1, indicating that equal importance is given to all data points.

Efficiency measurements were carried out by setting the cell to 2 V. The hydrogen produced was collected in a 50 ml gas burette equipped with a levelling bulb. Gas collection was carried out over 60 seconds. Data was averaged over 4 repetitions and gas volumes were corrected for temperature and barometric pressure. Energy efficiencies were calculated on the basis of the higher heating value of hydrogen.[30]

Scanning electron microscopy

Scanning electron microscopy was performed with a Philips XL30 ESEM instrument equipped with an Oxford Instruments Energy 250 energy dispersive spectrometer system at an acceleration voltage of 25 kV. Samples were loaded into the instrument on 25 mm AGAR scientific conductive carbon tabs. Images were obtained with acceleration voltages 25 kV and images were collected using Oxford Instrument INCA 4.09 Microanalysis Suite – Issue 17b.

Conclusions

We have demonstrated that a viable, practical electrochemical device can be fabricated using a 3D printer and appropriate surface coatings. The potential for rapid prototyping should allow for exploitation of the optimal flow plate geometries for a given device. The reduction in cost and weight should prompt further exploration of the potential of renewable hydrogen production and use in applications demanding such properties. Further work in this area will include extension of the application of 3D printing to other electrochemical devices, *e.g.* fuel cells and the further investigation of different materials and coating methodologies.

Acknowledgements

We would like to thank Margaret Mullin for the preparation of the sputter coated layers for the anode, the EPSRC (grants EP/H024107/1; EP/I033459/1; EP/J015156/1), WestCHEM and the University of Glasgow for funding this work. LC also thanks the Royal-Society Wolfson Foundation for a Merit Award.

Notes and references

1 D. Hissel, M.-C. Pera, H. Gualous and C. Turpin, *Electrochemical Components*, Wiley, United Kingdom, 2013.
2 B. Bensmann, R. Hanke-Rauschenbach, I. K. Peña Arias and K. Sundmacher, *Electrochim. Acta*, 2013, **110**, 570–580.
3 F. Barbir, *Sol. Energy*, 2005, **78**, 661–669.
4 M. Carmo, D. L. Fritz, J. Mergel and D. Stolten, *Int. J. Hydrogen Energy*, 2013, **38**, 4901–4934.
5 P. Millet, S. A. Grigoriev and V. I. Porembskiy, *Int. J. Energy Res.*, 2013, **37**, 449–456.
6 K. E. Ayers, E. B. Anderson, C. Capuano, B. Carter, L. Dalton, G. Hanlon, J. Manco and M. Niedzwiecki, *ECS Trans.*, 2010, **33**, 3–15.
7 K. E. Ayers, C. Capuano and E. B. Anderson, *ECS Trans.*, 2012, **41**, 15–22.
8 H.-Y. Jung, S.-Y. Huang, P. Ganesan and B. N. Popov, *J. Power Sources*, 2009, **194**, 972–975.
9 S. Siracusano, V. Baglio, A. Di Blasi, N. Briguglio, A. Stassi, R. Ornelas, E. Trifoni, V. Antonucci and A. S. Aricò, *Int. J. Hydrogen Energy*, 2010, **35**, 5558–5568.
10 (*a*) C. A. Reiser, US4826742A, 1989; (*b*) H. H. Voss and C. Y. Chow, US5230966, 1993; (*c*) F. R. Spurrier, B. L. Pierce and M. K. Wright, US4631239, 1986; (*d*) C. Y. Chow, B. Woznikzca and J. K. K. Chan, CA2274974, 1999.
11 A. Kazim, H. T. Liu and P. Forges, *J. Appl. Electrochem.*, 1999, **29**, 1409–1416.
12 S. Siracusano, A. Di Blasi, V. Baglio, G. Brunaccini, N. Briguglio, A. Stassi, R. Ornelas, E. Trifoni, V. Antonucci and A. S. Aricò, *Int. J. Hydrogen Energy*, 2011, **36**, 3333–3339.
13 X. Li and I. Sabir, *Int. J. Hydrogen Energy*, 2005, **30**, 359–371.
14 M. Geissler and Y. Xia, *Adv. Mater.*, 2004, **16**, 1249–1269.
15 J. Stampfl and R. Liska, *Macromol. Chem. Phys.*, 2005, **206**, 1253–1256.
16 B. Y. Ahn, E. B. Duoss, M. J. Motala, X. Guo, S.-I. Park, Y. Xiong, J. Yoon, R. G. Nuzzo, J. A. Rogers and J. A. Lewis, *Science*, 2009, **323**, 1590–1593.
17 F. Ilievski, A. D. Mazzeo, R. F. Shepherd, X. Chen and G. M. Whitesides, *Angew. Chem., Int. Ed.*, 2011, **50**, 1890–1895.
18 S. A. Morin, R. F. Shepherd, S. W. Kwok, A. A. Stokes, A. Nemiroski and G. M. Whitesides, *Science*, 2012, **337**, 828–832.
19 T. Hasegawa, K. Nakashima, F. Omatsu and K. Ikuta, *Sens. Actuators, A*, 2008, **143**, 390–398.

20 M. D. Symes, P. J. Kitson, J. Yan, C. J. Richmond, G. J. T. Cooper, R. W. Bowman, T. Vilbrandt and L. Cronin, *Nat. Chem.*, 2012, **4**, 349–354.
21 P. J. Kitson, M. H. Rosnes, V. Sans, V. Dragone and L. Cronin, *Lab Chip*, 2012, **12**, 3267–3271.
22 P. J. Kitson, M. D. Symes, V. Dragone and L. Cronin, *Chem. Sci.*, 2013, **4**, 3099–3103.
23 B. J. Polk, A. Stelzenmuller, G. Mijares, W. MacCrehan and M. Gaitan, *Sens. Actuators, B*, 2006, **114**, 239–247.
24 B. Domenech, M. Munoz, D. N. Muraviev and J. Macanas, *Chem. Commun.*, 2014, **50**, 4693–4695.
25 Metalprices.com, http://www.metalprices.com/metal/titanium/titanium-grade-1-slab-rotterdam, accessed May 2014.
26 Platts Global Petrochemical Index, http://www.platts.com/news-feature/2012/pgpi/polypropylene, accessed May 2014.
27 Bullionvault, http://www.bullionvault.com/silver-price-chart.do.
28 G. W. C. Kaye and T. H. Laby, *Tables of physical and chemical constants and some mathematical functions*, Longman, 1986.
29 W. M. Haynes and D. R. Lide, *CRC Handbook of Chemistry and Physics: A Ready-reference Book of Chemical and Physical Data*, CRC Press, 2011.
30 R. R. K. W. Harrison, G. D. Martin and A. Hoskin, *Hydrogen Production: Fundamentals and Case Study Summaries*, Report NREL/CP-550–47302, Oak Ridge, TN, USA, 2010.